

Submitted to the Astronomical Journal

# A Catalog of 1022 Bright Contact Binary Stars

S. J. Gettel<sup>1,2</sup>, M. T. Geske<sup>1</sup> and T. A. McKay<sup>1</sup>

## ABSTRACT

In this work we describe a large new sample of contact binary stars extracted in a uniform manner from sky patrol data taken by the ROTSE-I telescope. Extensive ROTSE-I light curve data is combined with J, H, and K band near-infrared data taken from the Two Micron All-Sky Survey (2MASS) to add color information. Contact binaries candidates are selected using the observed period-color relation. Candidates are confirmed by visual examination of the light curves. To enhance the utility of this catalog, we derive a new  $J-H$  period-color-luminosity relation and use this to estimate distances for the entire catalog. From these distance estimates we derive an estimated contact binary space density of  $1.7 \pm 0.6 \times 10^{-5} \text{ pcs}^{-3}$ .

*Subject headings:* binaries: close — catalogs — stars: variables: other

## 1. INTRODUCTION

W UMa-type contact binaries are eclipsing systems in which both stars overflow their Roche lobes, forming a common envelope of material (Lucy 1968). They are formed from nearly normal main-sequence stars with spectral types usually between F and K. Typical mass ratios are between  $q \approx 0.2 - 0.5$ , but reported values are almost as high as unity, and as low as 0.066 (Rucinski, et al. 2001). Their periods range from 0.22 days to 1.5 days, with most systems having periods between 0.25 – 0.5 days. Because of their close proximity, they produce continuously varying light curves, making them detectable at a large range of inclinations.

Due to the common atmosphere, both stars have essentially the same surface temperature. Through a combination of Kepler's third law and the radius-color relationship for

---

<sup>1</sup>Department of Physics, University of Michigan, Ann Arbor, MI 48109

<sup>2</sup>sjgttl@umich.edu

main-sequence stars, this common temperature leads to a period-color-luminosity relation (Rucinski (1994), Rucinski & Duerbeck (1997)). This relation, along with their ease of detection, make contact binaries useful tracers of distance and galactic structure, especially on small scales (Rucinski 2004).

Contact binaries are known to be quite common among variable stars, though their space density is still debated. Early estimates range from  $10^{-6} \text{ pc}^{-3}$  (Kraft 1967) to  $10^{-4} \text{ pc}^{-3}$  (van’t Veer 1975). More recent estimates include those of Rucinski (2002), who found a density of  $1.0 \times 10^{-5} \text{ pc}^{-3}$ , or 1/500 main-sequence stars, in the solar neighborhood. This conflicts with a previous estimate of 1/130 main-sequence stars made using OGLE-I data in the galactic disk (Rucinski 1998b), and may be an indication of significant variability in the contact binary fraction through the galaxy.

Currently, the GCVS (Samus et al. 2004) labels 845 stars as EW type variables; W UMa variables with periods less than 1 day and nearly equal minima. However, GCVS classifications are not entirely secure. Other contact binary catalogs include that of Pribulla, et al. (2003), which contains 361 galactic EW and EB type variables, each previously identified by another catalog such as the GCVS. Contact binaries included had either light curve or good spectroscopic data available. Also, analysis of the ROTSE-I variability test fields (Akerlof, et al. 2000) found 382 contact binary candidates within about  $2000 \text{ deg}^2$ , identified by their light curve shape and period. Periods and light curve data were provided for all of these ROTSE-I objects.

We present here a catalog of 1022 contact binary stars, 836 of which are not found in the GCVS, SIMBAD database, Pribulla catalog or ROTSE-I test fields. Light curve data, periods, and distance estimates are presented for each object. These objects passed a rather stringent selection process and have high quality light curves, so their classification is relatively secure. The completeness of this catalog for the regions surveyed is estimated to be about 34%, with the remaining objects lost to data quality cuts. Near infrared observations of these objects drawn from the Two-Micron All-Sky Survey (2MASS) allow us to create a NIR period-color-luminosity relation and to estimate distances to each object. Finally, an estimate of the space density of these objects is made.

Section 2 contains an overview of the data and selection methods, which is followed by a description of the method used to obtain distance estimates in Section 3. The space density derived from this catalog is discussed in Section 4. Section 5 contains a summary of the results.

## 2. ASSEMBLING THE CONTACT BINARY CATALOG

In this section we describe how we assemble a catalog of bright contact binary stars for study. We begin with a short description of the ROTSE-I instrument, which obtained the data, and the NSVS database on which this project is based. This is followed by a description of variable selection, identification of short period variables, phasing of these variables, combination of ROTSE-I optical data with 2MASS near-infrared data, and finally the selection of contact binaries from this catalog.

### 2.1. NSVS Data

Optical variability data were obtained by the ROTSE-I robotic telescope<sup>1</sup>. ROTSE-I was a four-fold array of Canon 200 mm f/1.8 lenses, each equipped with an unfiltered 2048x2048 pixel Thompson TH7899M CCD. At this f-number, the  $14\ \mu\text{m}$  pixels of the CCD subtend  $14.4''$  on the sky. The combined array imaged a continuous  $16^\circ \times 16^\circ$  field of view. ROTSE-I, designed to pursue real-time observations of gamma-ray bursts, spent most of the time from March 1998 until December 2001 patrolling the sky. The very large ROTSE-I field of view allowed it to image the entire available sky twice each night, taking a pair of 80 s images during each visit. Typical limiting magnitudes range from  $m_v = 14.5 - 15.5$ , depending on sky conditions. During its operating life, ROTSE-I amassed a 7 terabyte time domain survey of the night sky. Since being disassembled in 2002, the ROTSE-I lens and camera assemblies have been reborn as elements of the Hungarian Automated Telescope Network (HAT-net; Bakos, et al. (2004)).

Initial studies of ROTSE-I sky patrols were reported in Akerlof, et al. (2000). Though this work examined only three months of observations covering just 5% of the sky patrol area it revealed nearly 1800 bright variable objects, most of which were previously unknown. More recently, light curve data from a full year of all ROTSE-I sky patrols has been released publicly by Wozniak, et al. (2004) as the Northern Sky Variability Survey (NSVS), which is available through the SKYDOT website at Los Alamos National Lab ([skydot.lanl.gov](http://skydot.lanl.gov)). This work includes the entire region north of  $-30^\circ$  declination, though coverage is neither perfectly uniform nor absolutely complete. Many more light curve points are available for sources at high declination than at low. Completeness is reduced in regions of very high stellar density.

All optical light curves used in this paper are drawn from the NSVS. Details of the SExtractor (Bertin & Arnoud 1996) based reductions and relative photometry corrections

---

<sup>1</sup>For more information about ROTSE see <http://www.rotse.net>

of ROTSE-I data for inclusion in the NSVS catalog, along with maps of source density and number of good light curve data points, are presented in Wozniak, et al. (2004).

## 2.2. Selection and Phasing of Variable Objects with Short Periods

Selection of variable objects from the NSVS light curve database follows the methods outlined in Akerlof, et al. (2000). For each object, available data are examined for all good coincident pairs of observations. For this purpose, ‘good’ points were defined at two levels, one more tolerant than the other. Cuts are made by examining the measurement flags described in Wozniak, et al. (2004). Our tight cuts require no processing flags except the SExtractor ‘blended’ flag, indicating that an object is the result of a deblending procedure. In addition to the ‘blended’ flag, our second set of loose cuts allow the inclusion of points that have ‘nocorr’ and ‘patch’ flags, indicating that the relative photometry correction of an object could not be estimated, or that the map of corrections was patched to obtain the value for that object. Both sets of cuts are quite restrictive and leave us with a set of very well measured light curves.

For each object with at least 20 pairs of observations passing the tolerant cuts, we calculate the modified Welch-Stetson (Welch & Stetson 1993) variability index  $I_{val}$  described in Akerlof, et al. (2000). The distribution of variability indices seen in a representative sample of the data is shown in Figure 1. This distribution is roughly Gaussian with a mean value of 0.227 and a width  $\sigma = 0.11$ . Every object with  $I_{val}$  greater than one, about  $7\sigma$  from the mean, is accepted as a variable. From a list of  $1.43 \times 10^7$  input light curves, 63665 are selected as variable by these criteria, a variability fraction of 0.45%. The total number of detectable variables, as can be seen from the  $I_{val}$  distribution plot, is substantially larger.

Most of the variable objects we identify are long period variables, with periods of 10 days or more. To identify short period variables within this set, we calculate a simple light curve roughness parameter similar in spirit to the WS variability parameter. For this calculation we consider triplets of consecutive pairs of observations spaced by no more than five days. For each of the outer pairs in a triplet we calculate the mean magnitude. Using these, we predict, by linear interpolation, the mean magnitude for the middle pair. We then compare the residual between actual and predicted magnitude for each observation in the central pair to the error in its magnitude.

$$\delta_1 = \frac{m_1 - m_{predicted}}{\sqrt{\sigma_1^2 + 0.04^2}} \quad (1)$$

$$\delta_2 = \frac{m_2 - m_{predicted}}{\sqrt{\sigma_2^2 + 0.04^2}} \quad (2)$$

An additional uncertainty of 0.04 magnitudes is added in quadrature to the measurement errors to reduce the sensitivity of this parameter to small non-Gaussian errors. We then sum the absolute values of the products of these scaled residuals, divided by the number of predicted points, to construct our roughness parameter:

$$R = \frac{1}{\sqrt{N_{\text{triplets}} \times (N_{\text{triplets}} - 1)}} \sum_{\text{triplets}} \sqrt{|\delta_1 \times \delta_2|} \quad (3)$$

The distribution of this roughness parameter for all of the 63665 variables is shown in Figure 1. For variables with periods longer than a few days, this roughness parameter is distributed in an approximately Gaussian manner, with a mean of 0.4 and a width  $\sigma = 0.22$ . To construct a list of candidate short period variables we select those with  $R > 1.0$ . The total number of such candidates is 17,508.

Each of these candidate short period variables is then passed to the cubic spline phasing code described in detail in Akerlof, et al. (1994). This code provides best-fit periods, period error estimates, and spline fit approximations for light curve shapes. For each variable, we test the quality of this phasing by measuring an analogous roughness parameter for the phased light curve. For most eclipsing systems the period identified is actually half the real period. If the light curve is symmetric (as is the case for full contact binaries), the phased light curve is very smooth with this period. If the minima are not symmetric, the light curve will appear ‘rough’ with this period, but smooth when tested at twice the period. As a result we measure light curve smoothness for both the identified period and for twice the period, and accept as well phased light curves which have acceptably small roughness with either period. Examples of this are shown in Figure 2. Comparison of this folded roughness to the original roughness allows us to define a sample which is well-phased. Of the 17,508 short period candidates, 16548 have a phased roughness parameter less than 1.5 when phased at either the derived period or twice the derived period. These objects are deemed to be confidently phased.

### 2.3. Combination of NSVS and 2MASS data

ROTSE-I data is unfiltered, so although we have excellent light curve information, we have no color information. To ameliorate this, we combine the ROTSE-I light curve information with J, H, and K band near-infrared data drawn from the Two Micron All-Sky Survey (2MASS). This combination is especially apt because 2MASS data is significantly deeper than ROTSE-I data. As a result 2MASS measurements for all ROTSE-I objects are rather precise.

2MASS observations are taken simultaneously in all three bands, and are reported for a single epoch. Combining these data with ROTSE information provides three colors,  $m_{ROTSE}$ -J, J-H, and H-K, where  $m_{ROTSE}$  is the mean apparent magnitude in the unfiltered ROTSE-I band. Color-color plots for all variables and for short period variables are shown in Figures 3 and 4. The 2MASS observations correspond to random phases of the ROTSE light curves, generating uncertainty in each value of  $m_{ROTSE}$ -J and causing the horizontal spread in the  $m_{ROTSE}$ -J v. J-H plots. The J-H and H-K color measurements do not suffer this dispersion, and the measured J, H, and K magnitudes can be simply compared to determine single epoch object colors.

To identify the proper 2MASS counterparts we pass the positions of all NSVS variables to the 2MASS database query tool at IPAC<sup>2</sup>. Since ROTSE-I pixels are relatively large, there can be minor ambiguity in the identification of the correct corresponding 2MASS source. This problem is limited by the fact that ROTSE-I variables are all rather bright and hence their sky density is not especially high. When there is more than one match, the chosen 2MASS matching object is the nearest object with  $m_{ROTSE} - J > 0$ .

Color-color plots for all the variables and those identified as short period by the methods described above are shown in Figures 3 and 4. It is clear by comparison that the short period candidates are a special, predominantly blue, subset. Visual examination of the few red ( $m_{ROTSE} - J > 3.0$ ) short period candidates shows them to all be long period variables with relatively large light curve roughness. As a result, we further refine our short period variable candidate list by requiring  $m_{ROTSE} - J \leq 3.0$  and  $H - K \leq 0.35$ . These cuts leave a total of 16046 phased short period variable candidates.

## 2.4. Selection of Contact Binary Stars

Contact binary stars are known to exhibit a period-color relation. As shown in Figure 5, there is a dense patch of short period variables which displays a period-color dependence. Comparison to the location in period-color space of known contact binaries suggests that this excess is largely due to these stars. To generate a list of potential contact binaries, cuts were made defining the region:

$$0.26 < \Gamma < 0.6 \tag{4}$$

$$0.71 - 1.45\Gamma < J - H < 0.96 - 1.45\Gamma \tag{5}$$

---

<sup>2</sup><http://www.ipac.caltech.edu/2mass/>

selecting a total of 5179 objects. Here, the period ( $\Gamma$ ) is twice the value returned by the phasing procedure, and so represents the true period for contact binaries.

Interspersed throughout the region of period-color dependence is a background of variables which are not contact binaries. Upon scanning the light curves, many of the 5179 candidates were found to be other types of variables. In addition, many of the candidates with lower  $I_{val}$  parameters had small-amplitude light curves and large photometry errors, making classification difficult.

To ensure an essentially pure sample of contact binaries, further data quality cuts were made to select only the very well measured light curves. A cut at  $I_{val} > 2$  eliminated 62% of candidates, many of which had relatively indistinct light curves. An additional cut was placed on the roughness of the light curve when phased at the true period, requiring this to fall in a range from 0.25 to 0.75. This removed an additional 14% of the candidates, mostly variables which were clearly not contact binaries and so had light curves characterized by a different phased roughness value. The remaining 1238 candidates were individually scanned and 66 objects that did not appear to be contact binaries were removed. 9 of these appeared to be RR Lyrae stars and 3 appeared to be ordinary eclipsing binaries. The other removed light curves were not sufficiently well measured to be easily identified and many appeared to have asymmetric brightening and dimming phases. After these cuts, a sample of 1172 contact binaries remains.

Finally, due to the overlap in the fields, some of the objects appear two or more times in the catalog. In these cases we kept in the catalog data from the field that provided the most good observations. After discarding the duplicate objects, we are left with a catalog of 1022 contact binaries. Based on visual inspection and comparison to existing catalogs we expect this sample to be rather pure, with perhaps 5% contamination of pulsating variables such as RRc stars. A sample of this catalog is given in Table 1. The full catalog is available online.

## 2.5. Tests of Selection Efficiency

In this section we describe efforts to determine the selection efficiency for contact binaries. We test the catalog of Pribulla, et al. (2003) for inclusion in our catalog. Due to the data quality cuts, it is expected that our catalog will be most complete for nearby objects, but it is not possible to use a volume-limited sample, as their catalog does not contain distance estimates. Instead, we use a magnitude-limited sample, restricting our analysis of completeness to objects brighter than 12.5 magnitudes. This corresponds roughly to the

objects whose distance estimates placed them within 300 pcs. In the Pribulla catalog, there were 274 known contact binaries with maximum apparent magnitude values less than 12.5. A total of 148 of these were located within the NSVS survey region. Among these, 50 objects were included in the final catalog, resulting in a total completeness level of about 34%. This low efficiency reflects the stringent cuts made to ensure a pure sample.

The remaining objects were not included in the catalog for a variety of reasons. The 148 Pribulla stars that could reasonably have been observed were compared to the list of 16548 well-phased short period variables. There were 88 matches, about 25% of which fall outside of the period-color cuts we have defined. Another 20% do not pass the data quality cuts. The remaining 60 objects do not have enough good observations, either because they fall in regions of high stellar density (near the galactic plane) or because they are in regions less well observed in the NSVS.

### 3. ESTIMATING DISTANCES TO CONTACT BINARIES

In this section we describe the calibration of a near-infrared period, color, luminosity relation for contact binaries. We also discuss applying this relation to estimate distances to all of our contact binaries.

#### 3.1. Determining $V_{max}$

For contact binaries, the maximum magnitude  $V_{max}$  is independent of inclination, and hence is an appropriate measure of apparent magnitude for distance estimation. The  $V_{max}$  of each object was determined from its light curve. First, the light curves were phased, then the observations dimmer than the mean magnitude were removed and a parabola was fitted to the remaining points. The vertex of the parabola was taken to be the maximum magnitude. If the fit failed,  $V_{max}$  was taken to be the average magnitude of the brightest observations. Figure 6 shows the parabola fit used in obtaining  $V_{max}$  for eight random objects in the catalog.

To obtain the error on  $V_{max}$ , this fit was bootstrap re-sampled 10000 times. Of the  $N$  datapoints for each star, a random sample of size  $N$  was selected, creating numerous slightly different fits from a single light curve. The resulting distribution of  $V_{max}$  values was histogrammed using the optimal bin size and then fitted to a Gaussian. The mean of the Gaussian was taken to be  $V_{max}$  and its standard deviation was taken to be the error on  $V_{max}$ . Examples of the Gaussian fit to the histogram are given in Figure 7.



For most objects, the mean of the Gaussian differed by less than .1 magnitude from the median of the bootstrap distribution. However, in a few the difference was much larger. These objects also had atypically large standard deviation for their Gaussian fits. In this case,  $V_{max}$  values at  $4\sigma$  of the bootstrap distribution and beyond were thrown out, and the recalculated median and standard deviation were used as  $V_{max}$  and its uncertainty, respectively.

### 3.2. Calibrating the Period-Color-Luminosity Relation

To obtain distance estimates, a sample of 38 previously known contact binaries was used. Each of these objects has parallax data from the Hipparcos catalog, in addition to 2MASS color data and a period derived from its light curve. Reference distances were calculated from parallax, then three objects were removed due to poorly determined distance estimates. Absolute magnitude values were then determined from parallax.

Rucinski & Duerbeck (1997) established a relation between the period,  $B-V$  color and absolute magnitude of a contact binary system. Contact binaries are close to the main sequence and so have a mass-radius dependence. Because the stars are in contact, the period of the system depends on the radii of the component stars, so the color of the system depends on its period.

We derived a similar relation using the  $J-H$  color obtained by 2MASS. A plane was fitted to the period, color and luminosity data of the 35 calibration stars, which were weighted by distance uncertainty. The coefficients of this initial fit were sampled until a minimum value of  $\chi^2$  was found and these new coefficients were selected to be the proper fit. The uncertainty on these coefficients was derived from their pattern of variation with increasing  $\chi^2$ . The observed relation can be written:

$$M_{ROTSE} = (2.20 \pm 0.66) + (0.88 \pm 1.01) \log(\Gamma) + (7.99 \pm 2.33)(J - H). \quad (6)$$

Used in combination with the standard magnitude-distance formulas, we obtain the relation

$$\log(D) = 0.2V_{max} - 0.18 \log(\Gamma) - 1.60(J - H) + 0.56 \quad (7)$$

where distance is in parsecs and  $\Gamma$  is the true period in days. When used to calculate distances for our sample, all but about 23% had values within 80 pcs of their distances from parallax. The median difference was 36 pcs and the maximum was 273 pcs. The comparison between the calculated distance and the distance from parallax is shown in Figure 8. This relation was then used to obtain distance estimates for the full set of contact binaries.

### 3.3. Comparison to Other Calibrations

Rucinski and Duerbeck’s original period-color-luminosity relation was then applied to our calibration sample. Their absolute magnitude estimates tended to be lower and their distance estimates slightly higher than ours. See Figure 9. All but about 22% of their distance estimates were within 80 pcs of the references distances. The median difference was 39 pcs and the maximum was 400 pcs; results which are comparable to those obtained here. Rucinski and Duerbeck used a calibration sample of 40 systems, only slightly larger than ours. However, those systems have a larger range of period,  $0.24 < \Gamma < 1.15$  days versus  $0.24 < \Gamma < 1.06$ , and color,  $0.26 < B-V < 1.14$  versus  $0.28 < B-V < 0.87$ , than do the 31 systems in our calibration set for which  $B-V$  values are known. Therefore their calibration set may be more representative of the entire class of contact binaries.

### 3.4. Tests for Third Parameters

Earlier absolute magnitude calibrations have included additional dependences, such as the metallicity and the orbital inclination of the system. To test for sources of dispersion in the period-color-luminosity relation, the distance residuals were plotted against all available colors:  $m_{ROTSE-J}$ , J-H, H-K, and  $B-V$ ; as well as  $\Gamma$ ,  $V_{max}$ ,  $I_{val}$ , and the amplitude of the light curve. Any dependence on these last two parameters may be representative of a dependence on orbital inclination. Any relationship between the distance residuals and period or J-H would indicate that absolute magnitude depends more strongly on those parameters than the calculated period-color-luminosity relation suggests. However, no significant dependencies were found. See plots in Figures 10 and 11.

## 4. ESTIMATING THE SPACE DENSITY OF CONTACT BINARIES

The cumulative number of detections should increase with the distance to the sources cubed, if contact binaries are homogeneously distributed. To calculate the space density of contact binaries, we must first estimate the sky coverage of the contact binary catalog. We limit our analysis to the sky north of  $0^\circ$  declination, which was more thoroughly observed. This yields an area of  $17458 \text{ deg}^2$ , or about 42% of the sky. Therefore we take the total volume studied to be approximately  $0.55\pi d^3$ .

Using the distance estimates derived above and the method of Stepien, et al. (2001), a curve was fit to the cumulative number of contact binaries detected as a function of distance, using only objects from 150 to 300 parsecs. This is a distance range in which we expect

uniform completeness. As can be seen in Figure 12, the curve  $N = (9.9 \pm 3.7) \times 10^{-6}d^3$  gave a good fit over this distance range. This implies a measured space density of about  $(5.7 \pm 2.1) \times 10^{-6}pc^{-3}$ . However, the catalog is only about 34% complete for objects brighter than 12.5 magnitudes, which correspond approximately to those objects that are closer than 300 pcs, and thus used to determine the space density. Adjusting for this incompleteness, we obtain a space density of  $(1.7 \pm 0.6) \times 10^{-5}pc^{-3}$ . This agrees well with the recent estimate by Rucinski (2002), which was  $(1.02 \pm 0.24) \times 10^{-5}pc^{-3}$ .

## 5. CONCLUSION

In this work we present a new catalog of 1022 bright contact binary stars. All objects are selected from the extensive light curve database assembled in the Northern Sky Variability Survey from data taken from ROTSE-I sky patrol observations. Period, amplitude, light curve shape, and infrared colors are all used to identify contact binary candidates. We also present a period-color-relation using  $J-H$  and an estimate of the space density of contact binaries. The detection efficiency for contact binaries given the stringent set of cuts applied here was rather low, 34%. This suggests that as many as a few thousand more contact binaries remain to be extracted from the NSVS data set. In addition, tens of thousands of additional variable stars of all kinds remain to be extracted from this powerful resource.

This publication makes use of the data from the Northern Sky Variability Survey created jointly by the Los Alamos National Laboratory and University of Michigan. The NSVS was funded by the Department of Energy, the National Aeronautics and Space Administration and the National Science Foundation.

This publication also makes use of data products from the Two Micron All Sky Survey, which is a joint project of the University of Massachusetts and the Infrared Processing and Analysis Center/California Institute of Technology, funded by the National Aeronautics and Space Administration and the National Science Foundation.

ROTSE is supported at the University of Michigan by NSF grants AST 99-70818 and AST 04-07061, NASA grant NAG 5-5101, the Research Corporation, the University of Michigan and the Planetary Society. Gettel and Geske also acknowledge support from the University of Michigan REU site grant PHY 04-53355. Gettel is also supported by a Michigan Space Grant Consortium undergraduate research grant.

## REFERENCES

- Akerlof, C., et al., 1994, ApJ, 436, 787
- Akerlof, C., et al., 2000, AJ, 119, 1901
- Bakos, G., Noyes, R.W., Kovacs, G., Stanek, K.Z., Sasselov, D.D., & Domsa, I., 2004, PASP, 116, 266
- Bertin, E., & Arnoud, S., 1996, A&AS, 117, 393
- Kraft, R.P., 1967, PASP, 79, 395
- Lucy, L.B., AJ, 151, 1123
- Pribulla, T., Kreiner, J.M., & Tremko, J., 2003, CAOSP, 33,38
- Rucinski, S.M., 1994, PASP, 106, 462
- Rucinski, S.M., & Duerbeck, H.W., 1997, PASP, 109, 1340
- Rucinski, S.M., 1998b, AJ, 116, 2998
- Rucinski, S.M., Lu, W., Mochnacki, S.W., Ogloza, W., Stachowski, G., 2001, AJ, 122, 1974
- Rucinski, S.M., 2002, PASP, 114, 1124

- Rucinski, S. M. 2004, *New Astronomy Review*, 48, 703
- Samus, N. N., Durlevich, O. V., & et al. 2004, *VizieR Online Data Catalog*, 2250, 0
- Stepien, K., Schmitt, J.H.M.M., Voges, W., 2001, *A&A*, 370, 157
- van't Veer, F., 1975, *A&A*, 40, 167
- Welch, D., & Stetson, P. 1993, *AJ*, 105, 1813
- Wozniak, P., et al., 2004, *AJ*, 127, 2436

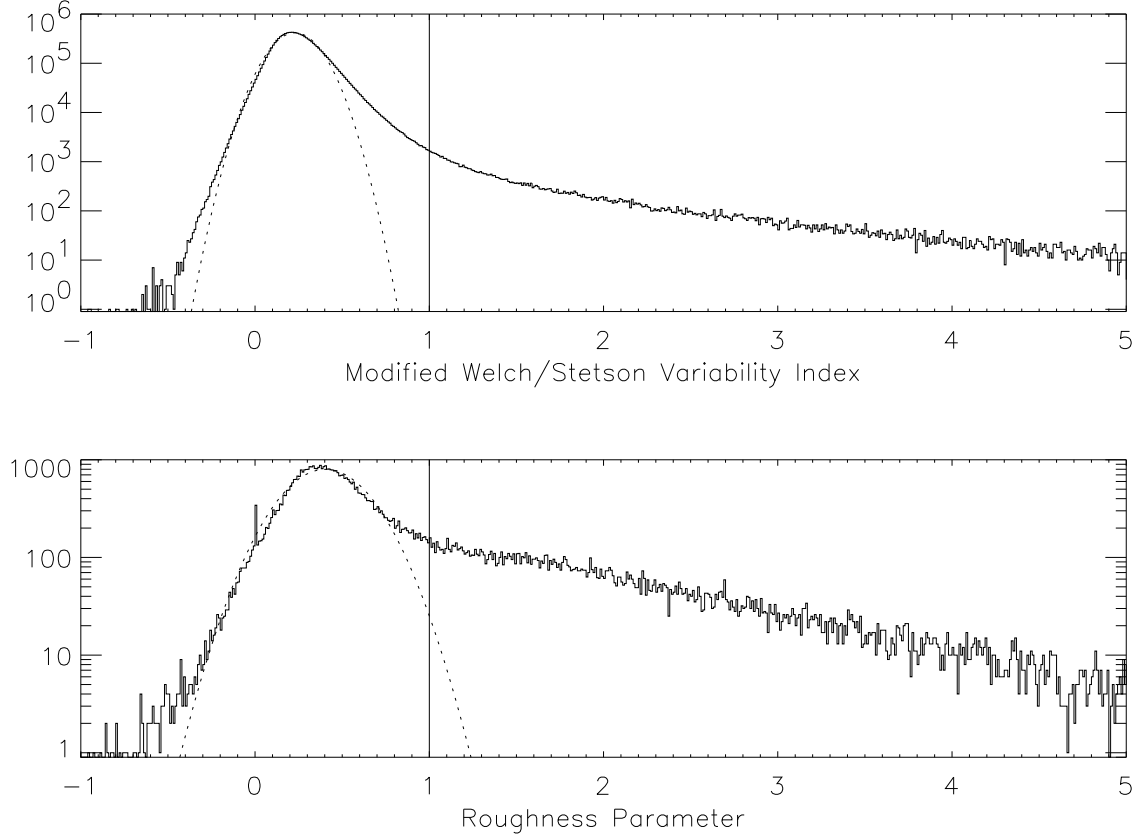


Fig. 1.— The figure on the top shows the distribution of modified Welch/Stetson variability indices for a representative subset of NSVS data. The dotted line shows a Gaussian fit to this distribution, and the solid line shows the variability cut (about seven  $\sigma$ ) applied in forming this catalog. The bottom figure shows the distribution of the roughness parameter  $R$  described in the text for the 63665 variables extracted from the NSVS light curve database. The dotted line shows a Gaussian fit to this distribution and the solid line shows the cut applied to identify short period variables.

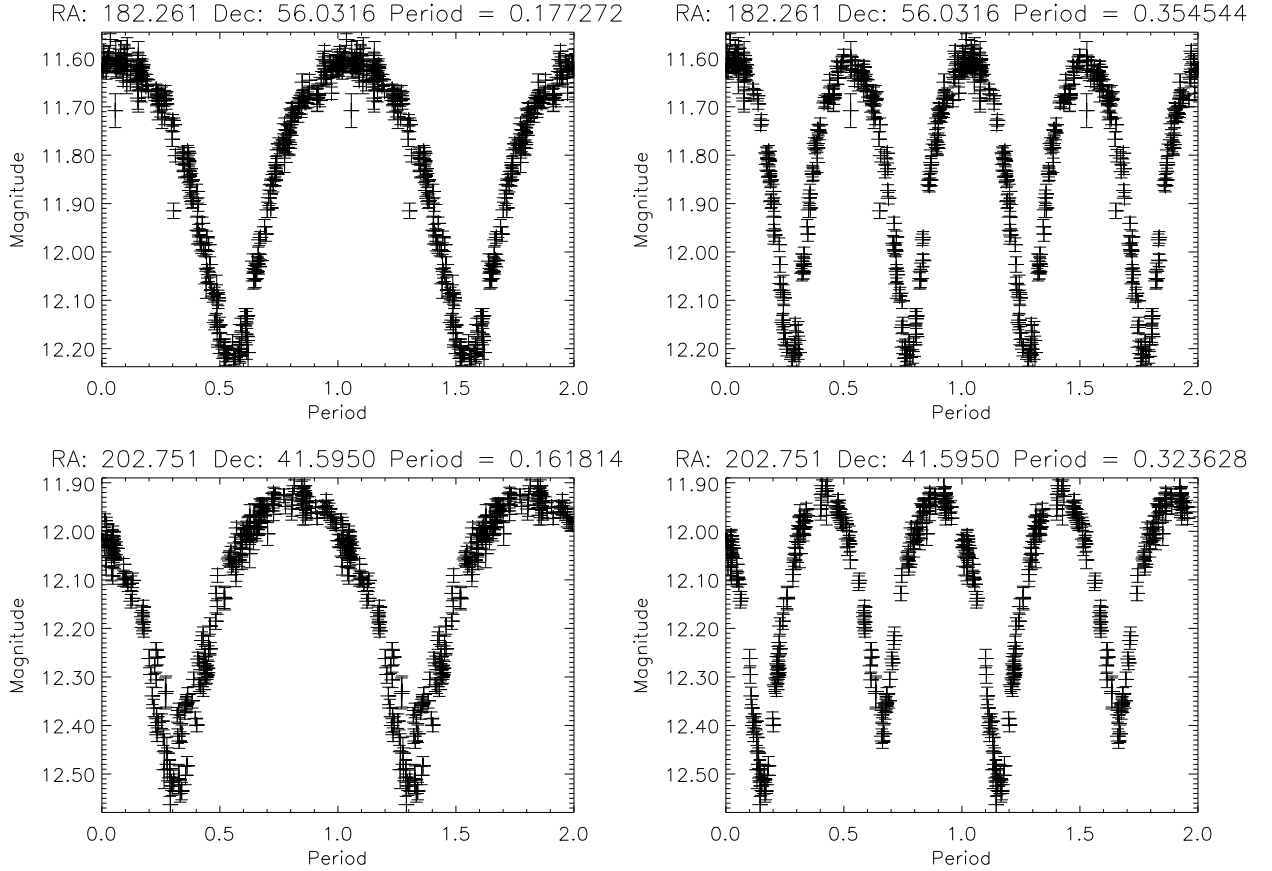


Fig. 2.— Phased light curves for two contact binary candidates. In cases where the light curve is fully symmetric, as in the top two panels, it appears smooth and single-valued when phased with half the real period (left) or with the full period (right). In cases where the minima are not identical, as in the bottom panels, the light curve looks multi-valued and ‘rough’ when phased at half the real period (left), but smooth when phased at the real period (right). In each case, data is repeated to show two full cycles of the light curve.

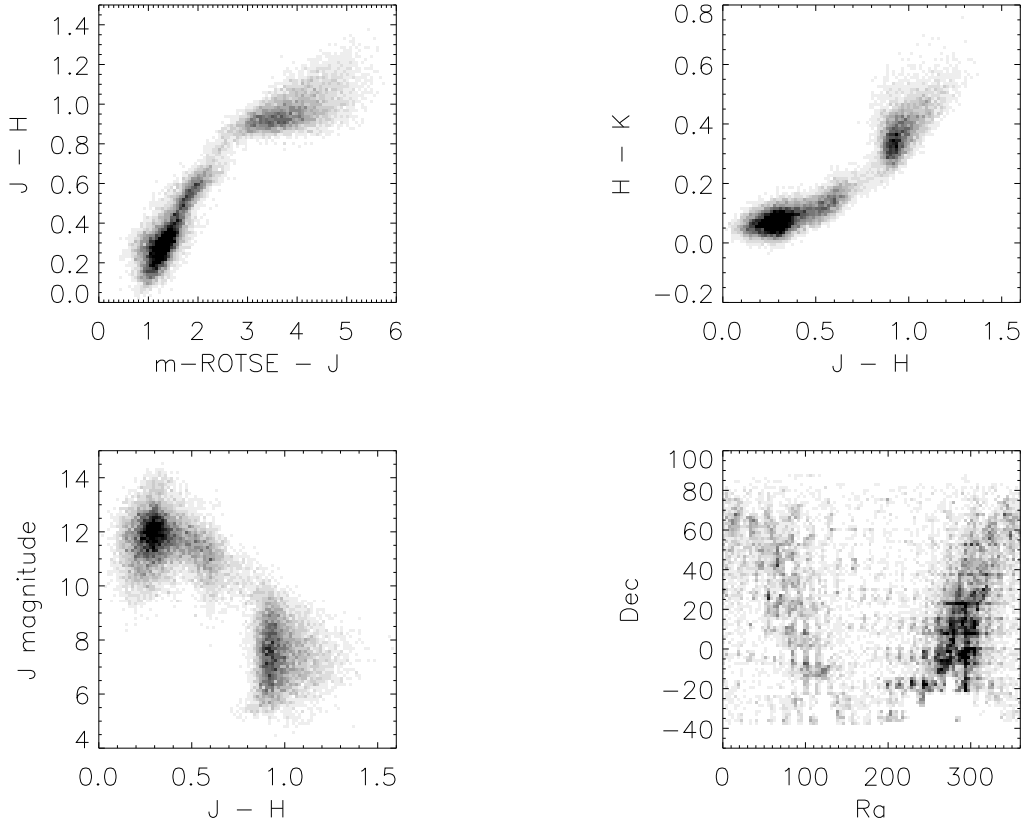


Fig. 3.— Color-color plots in  $m_{ROTSE} - J$ ,  $J - H$ , and  $H - K$  for all NSVS variables. The final panel shows an Aitoff projection of all objects.



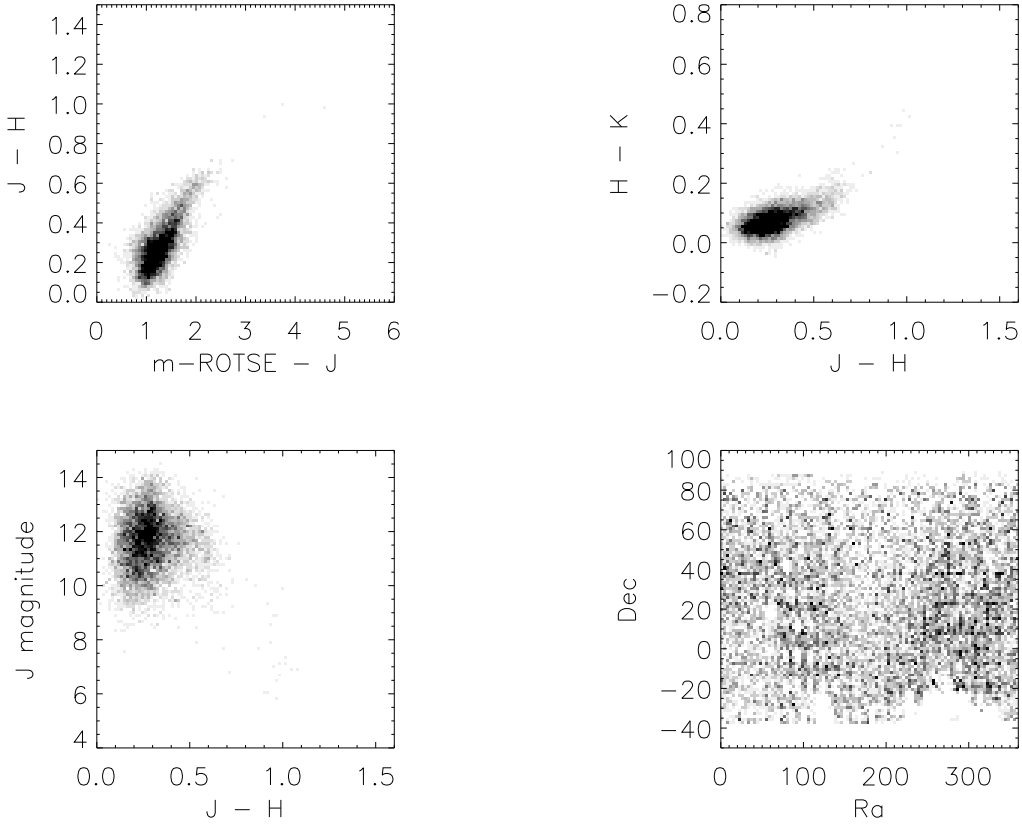


Fig. 4.— Color-color plots in  $m_{ROTSE} - J$ ,  $J - H$ , and  $H - K$  for those NSVS variables identified as potential short period variables by their light curve roughness. The final panel shows an Aitoff projection of all objects. It is clear from comparison to Figure 3 that the short period variables are drawn primarily from the blue population of stars.

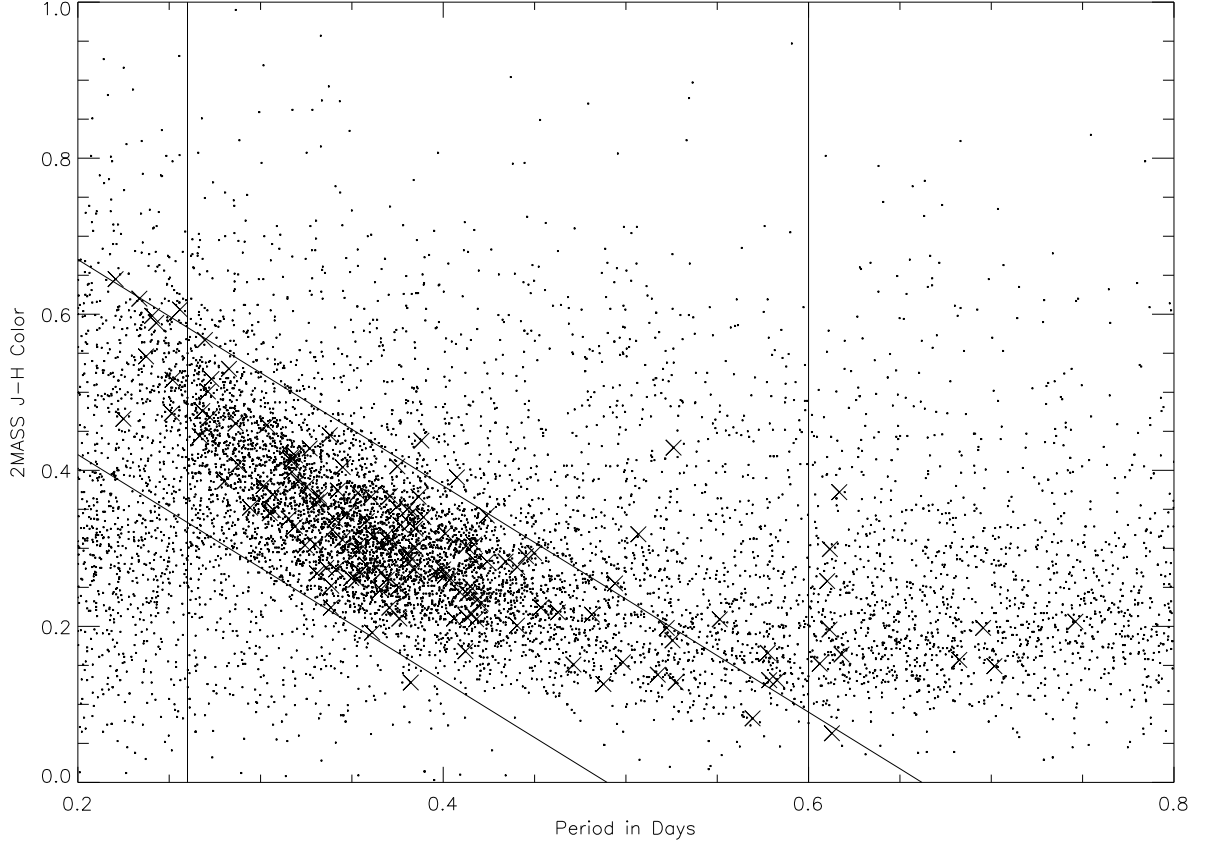


Fig. 5.— Period-color relation for the full short period variable sample (dots). A clear sequence of objects with the period-color dependence expected for contact binary stars stands out. We select as contact binary candidates all stars falling within the selection region shown. The known contact binaries from the catalog of Pribulla, et al. (2003) are also included (Xs).

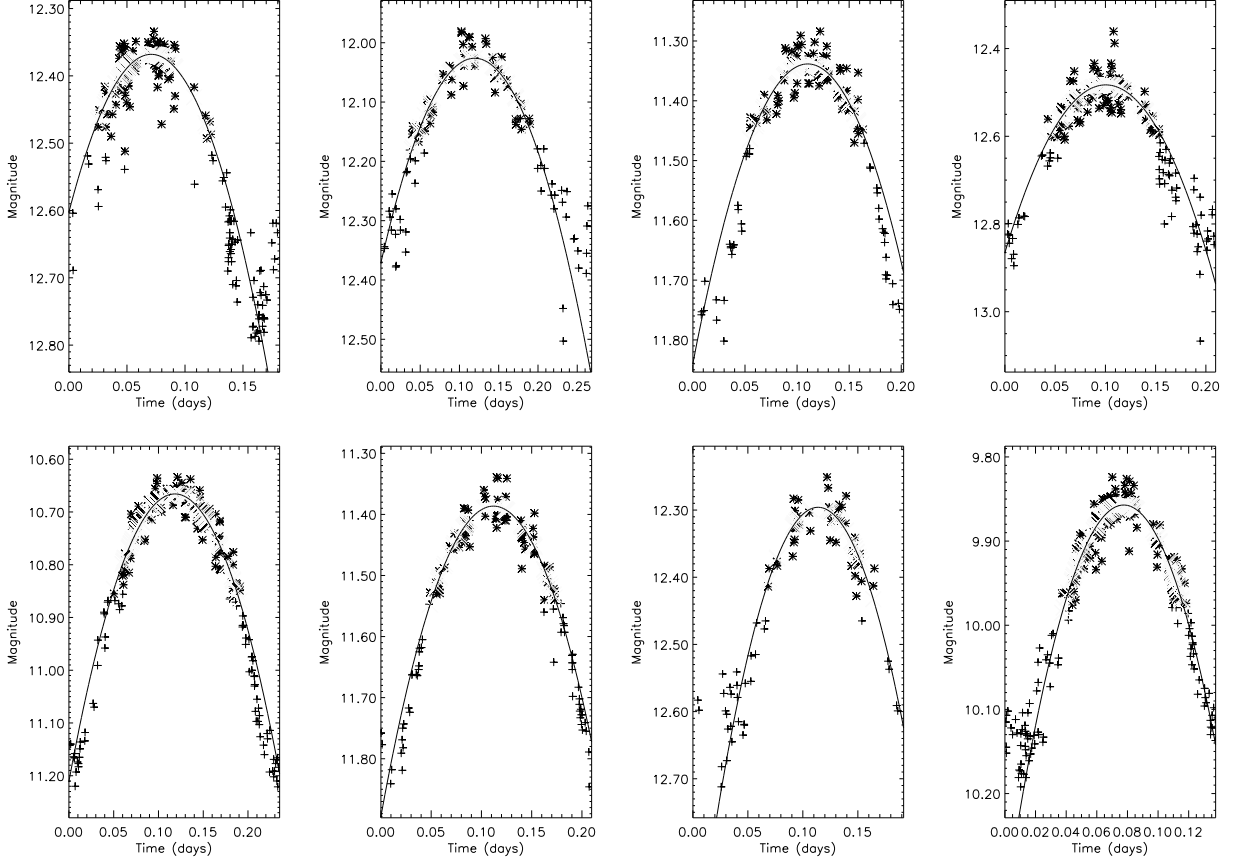


Fig. 6.— Examples of the automatic calculation of  $V_{max}$  for a random set of eight contact binaries.

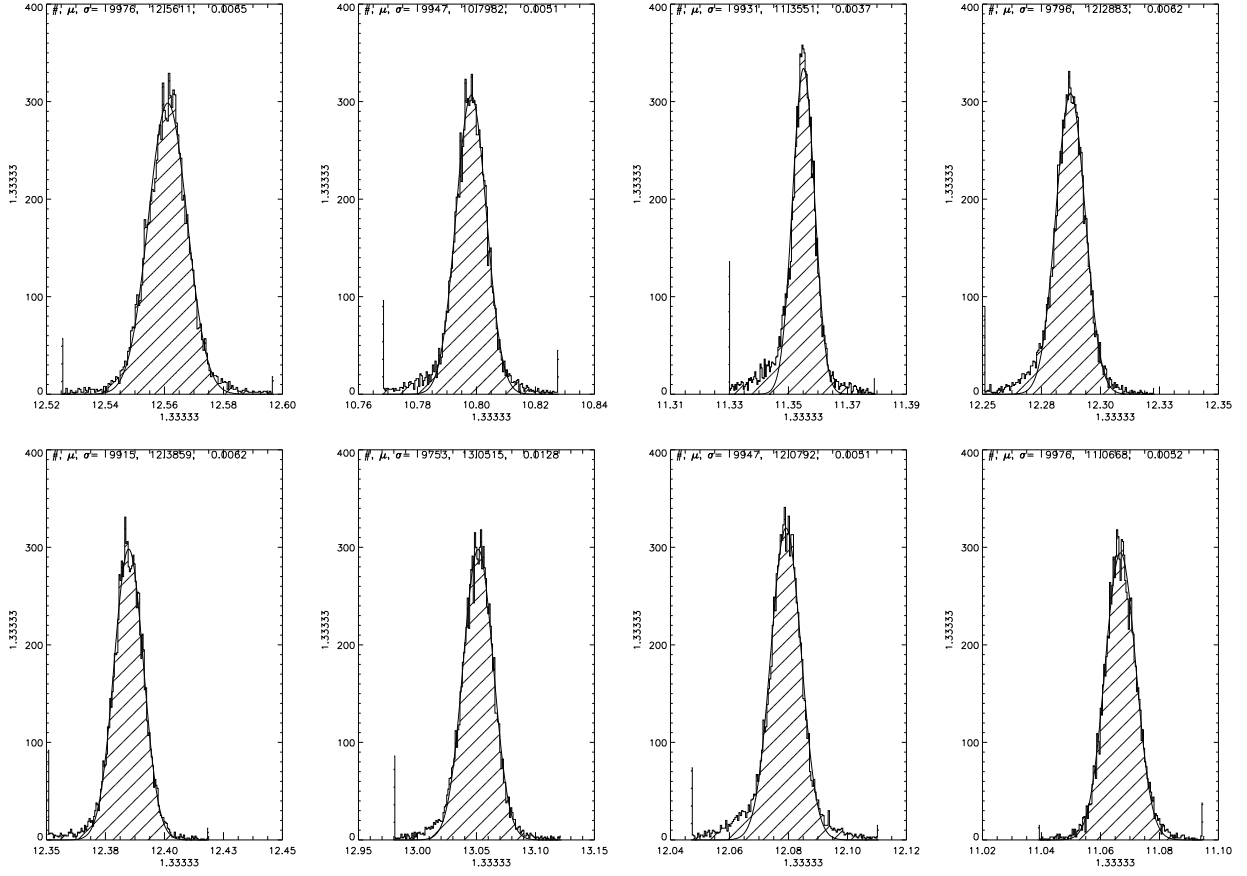


Fig. 7.— Examples of the Gaussian fit to the distribution of bootstrap re-sampled  $V_{max}$  values for a sample of eight contact binaries.

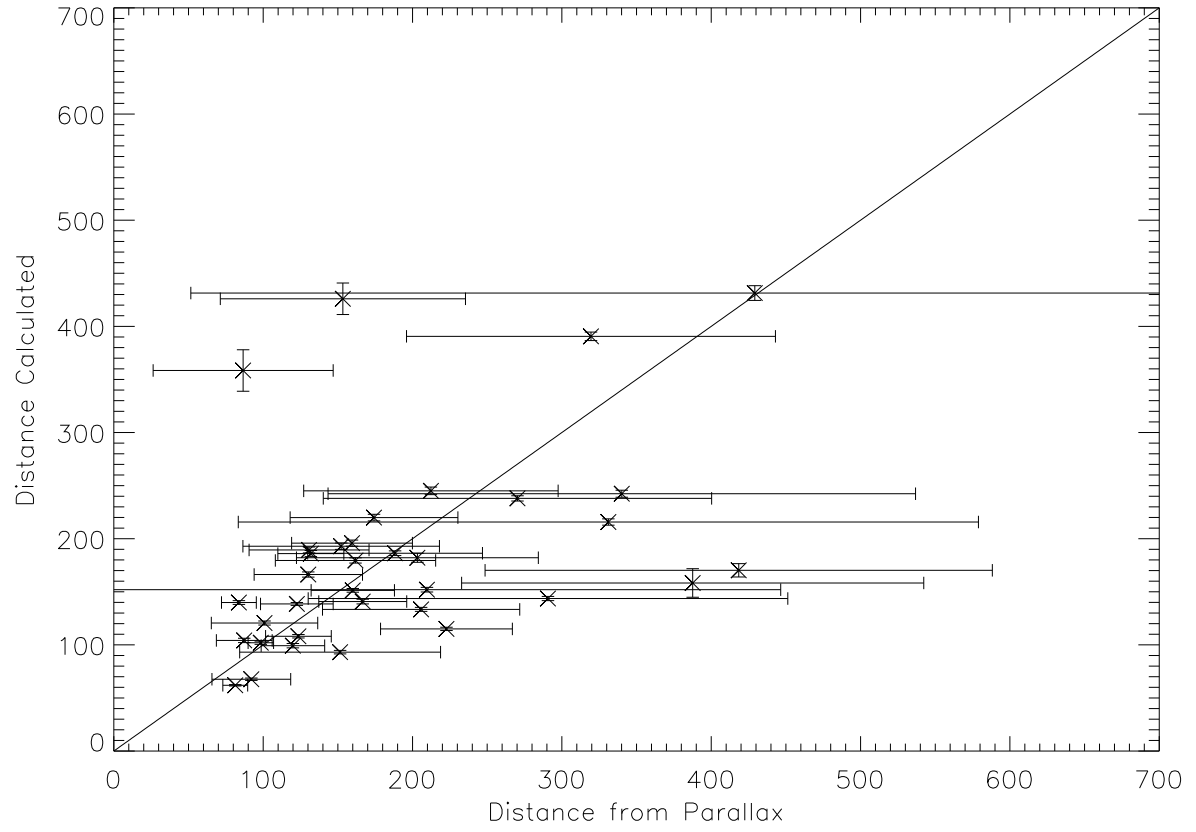


Fig. 8.— Distances (pcs) from parallax for the reference set of 35 contact binaries, against the distances obtained from the period-color-luminosity relation. Also included is a reference line of slope = 1.

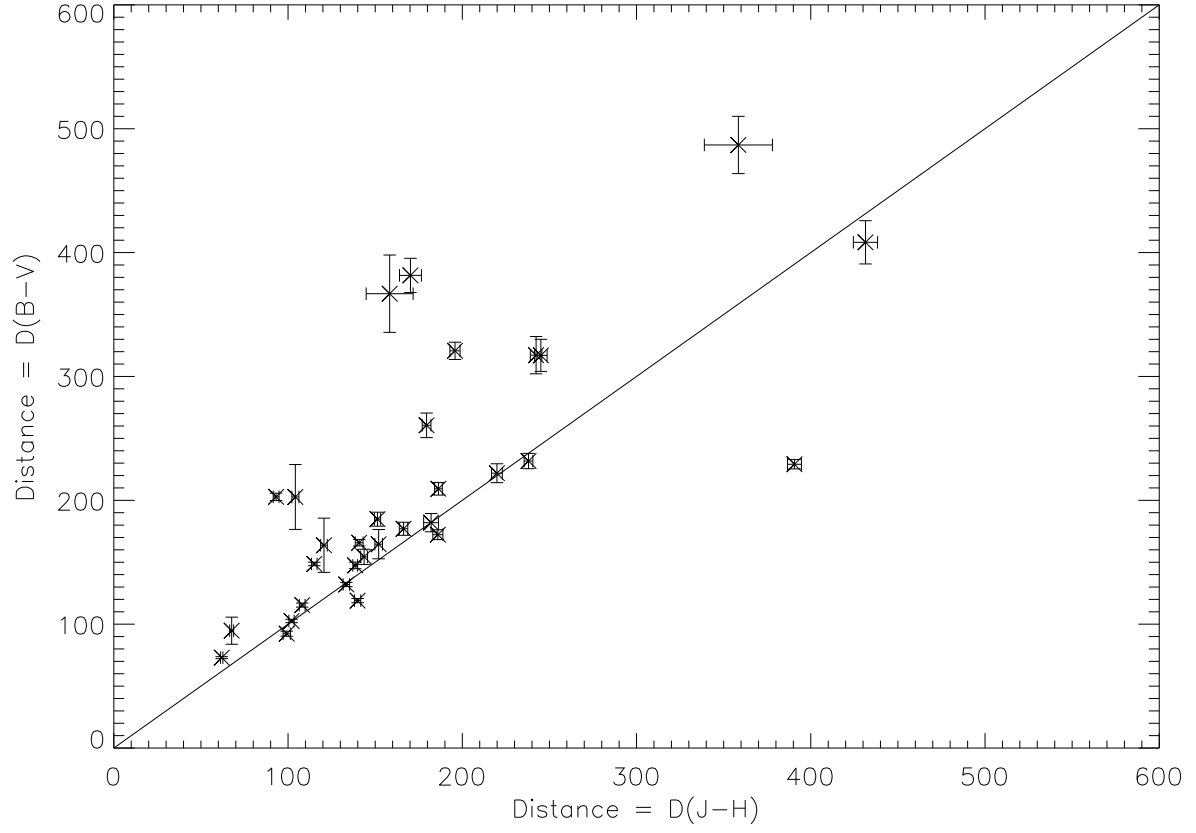


Fig. 9.— Distances (pcs) obtained from our period-color-luminosity relation for the reference set contact binaries, against their distances from that of Rucinski, in  $B-V$ . Also included is a reference line of slope = 1.

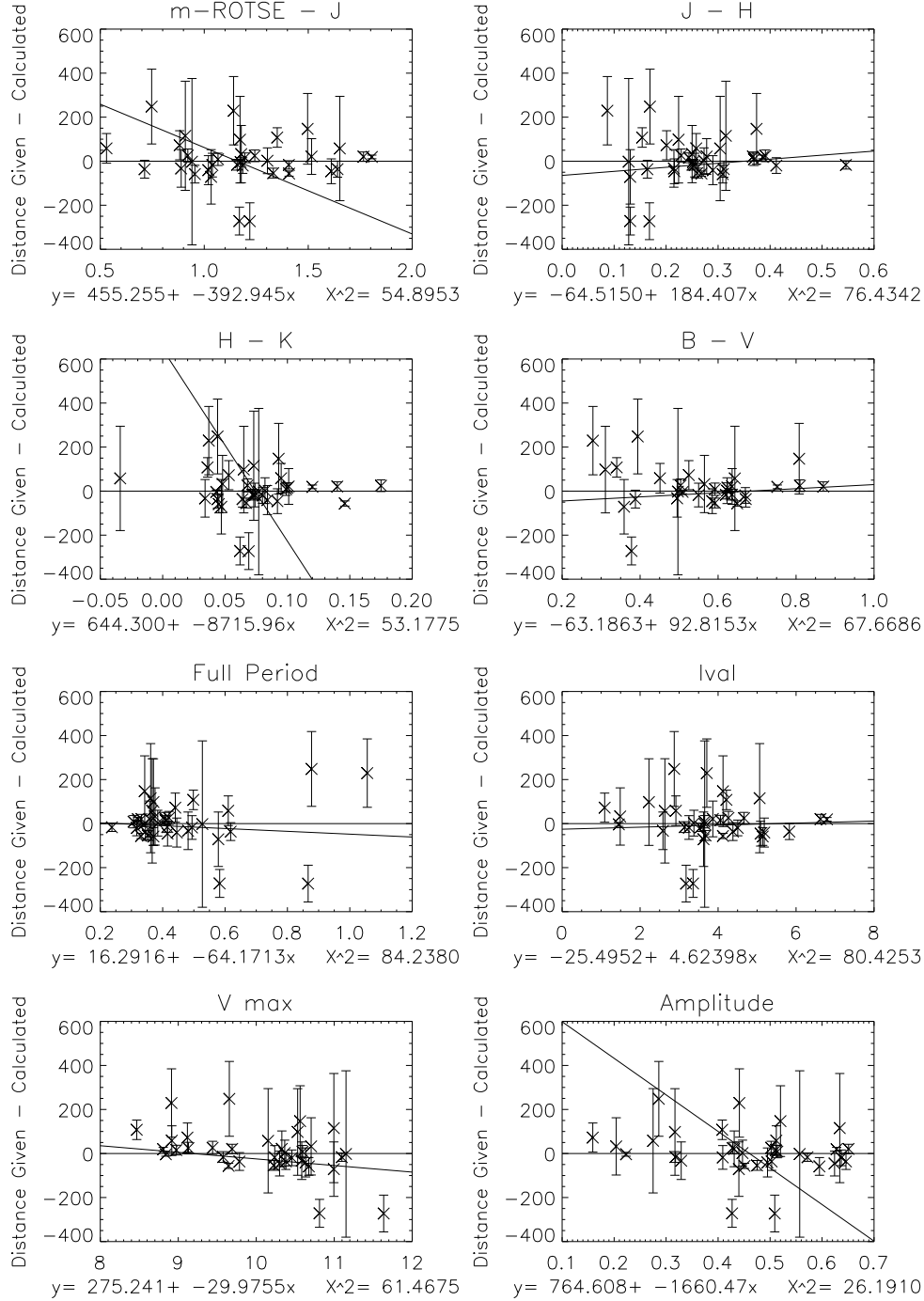


Fig. 10.— Residuals in distance from our period-color-luminosity relation. The included linear fits do not seem indicative of any real trend.

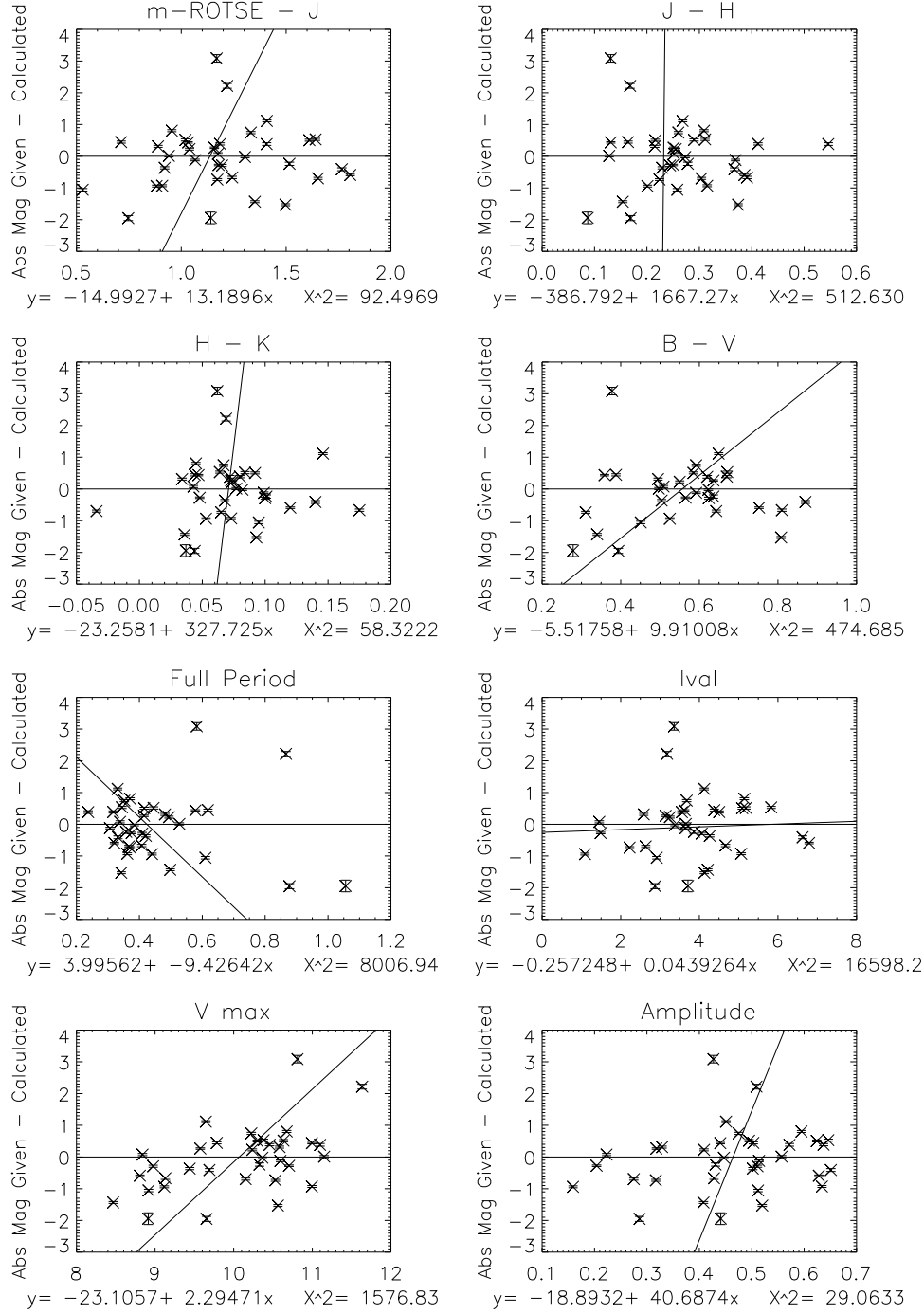


Fig. 11.— Residuals in absolute magnitude from our period-color-luminosity relation. The included linear fits do not seem indicative of any real trend.



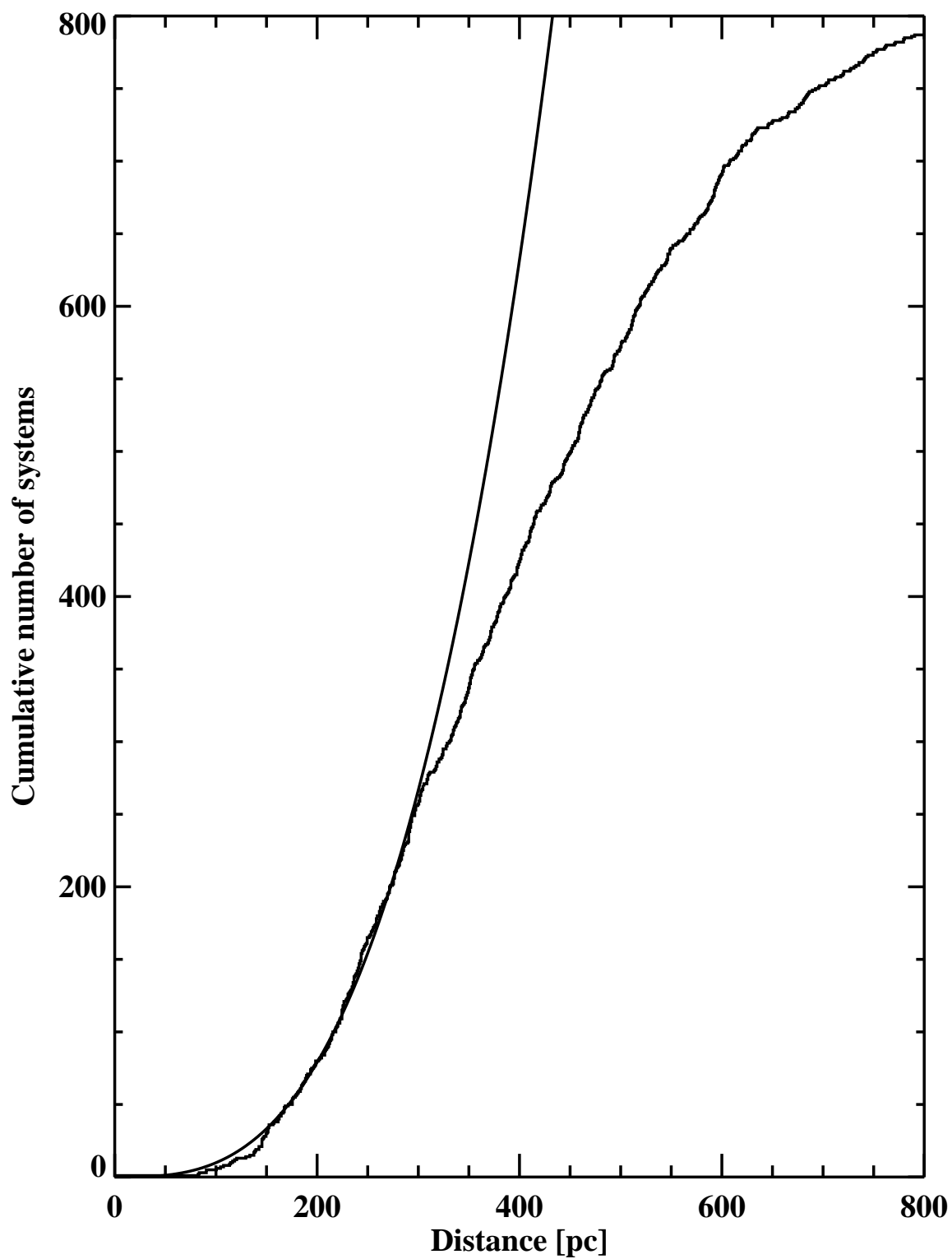


Fig. 12.— Cumulative number of systems plotted as a function of distance. The dashed curve represents the curve  $N = 9.9 \times 10^{-6} d^3$  systems per  $pc^3$ . The fit is very good out to about 300 pc.

Table 1. Properties of sample objects in the contact binary catalog <sup>a</sup>

ID	Ra	Dec	$m_R$	$m_R$ err	J	H	K	J err	H err	K err	$m_R$ -J	J-H	H-K	$\Gamma$	$V_{max}$	$V_{max}$ err	Max	Min	Amp	M	M err	D	D err	Field	Obs	GCVS Name	Ref
8711652	321.925	35.0875	12.659	0.27	11.179	10.84	10.747	0.017	0.016	0.006	1.48	0.339	0.093	0.334968	12.5618	0.0055	12.523	13.459	0.936	4.48844	0.025072	412	5	066a	319		
7604549	176.101	23.3565	12.092	0.266	10.295	9.837	9.726	0.018	0.018	0.014	1.797	0.458	0.111	0.303427	11.9309	0.00524	11.907	12.716	0.809	5.40103	0.026801	202	3	057b	279	CE Leo *	GC,PR
13267072	201.887	3.04122	11.212	0.261	9.693	9.396	9.28	0.018	0.021	0.02	1.519	0.297	0.116	0.353995	11.0426	0.004465	11.029	11.754	0.724	4.17416	0.029287	236	3	105d	213	AW Vir *	GC,PR
7726255	211.242	30.0006	11.619	0.285	10.306	10.002	9.934	0.02	0.023	0.015	1.313	0.304	0.067	0.324288	11.5106	0.003869	11.498	12.224	0.726	4.19645	0.031747	290	4	059b	212	TU Boo *	GC,PR,RT
14850169	53.9278	-20.352	11.847	0.271	10.233	9.898	9.845	0.019	0.02	0.019	1.614	0.335	0.052	0.327091	11.6192	0.007031	11.631	12.26	0.629	4.44737	0.029001	272	4	120b	188		
12142698	54.9961	3.24179	11.43	0.285	10.359	9.886	9.735	0.021	0.022	0.017	1.071	0.473	0.151	0.282723	11.3186	0.004425	11.307	12.067	0.76	5.49374	0.031427	146	2	096a	262		
12395130	87.4975	-7.4318	12.47	0.3	11.114	10.662	10.533	0.021	0.022	0.019	1.356	0.452	0.129	0.322597	12.305	0.006254	12.274	13.167	0.893	5.37661	0.031672	243	4	098b	243		
12310373	77.2155	2.82084	11.418	0.241	9.77	9.339	9.272	0.023	0.02	0.019	1.648	0.431	0.066	0.295713	11.2387	0.00477	11.236	11.88	0.644	5.17549	0.031565	163	2	097d	246		
7655121	188.771	23.3371	10.746	0.276	9.326	9.102	9.002	0.018	0.019	0.015	1.42	0.224	0.1	0.338505	10.5973	0.004076	10.594	11.257	0.663	3.5739	0.027753	254	3	058b	292	RZ Com *	GC,PR,RT
706127	109.27	77.1739	11.676	0.247	10.39	9.974	9.884	0.021	0.017	0.013	1.286	0.416	0.09	0.298445	11.5549	0.006201	11.536	12.23	0.693	5.05921	0.028256	199	3	005d	691		
9179857	17.3828	22.6553	11.396	0.254	10.303	10.13	10.077	0.019	0.02	0.018	1.093	0.173	0.053	0.494339	11.2792	0.004494	11.263	11.932	0.669	3.31178	0.031024	392	6	069d	318		
7463810	144.789	31.4129	12.15	0.248	10.624	10.314	10.235	0.02	0.021	0.016	1.526	0.309	0.079	0.358664	12.019	0.005425	12.014	12.645	0.631	4.28301	0.030596	353	5	055a	279		
1119084	258.558	76.704	11.255	0.245	9.541	9.133	9.033	0.018	0.014	0.013	1.714	0.408	0.1	0.325397	11.1248	0.004801	11.099	11.953	0.854	5.02846	0.024481	166	2	009d	689		
9216203	22.5684	13.557	11.18	0.251	9.659	9.289	9.215	0.018	0.031	0.016	1.521	0.37	0.073	0.324736	11.0303	0.003985	11.016	11.708	0.692	4.72416	0.036933	182	3	070b	295		
14887343	62.9492	-11.79	11.565	0.25	10.144	9.839	9.747	0.025	0.02	0.019	1.421	0.305	0.092	0.416889	11.4368	0.005135	11.423	12.148	0.724	4.30078	0.033995	267	4	120d	214	BL Eri *	GC,PR
269914	26.4939	80.0821	11.295	0.258	10.297	9.969	9.923	0.019	0.027	0.019	0.998	0.328	0.045	0.318828	11.1523	0.002926	11.131	11.785	0.654	4.38164	0.034154	226	4	002d	725	GW Cep *	GC,PR
13334244	213.254	6.94132	12.733	0.27	11.411	11.083	11.021	0.021	0.025	0.023	1.322	0.328	0.062	0.333536	12.6732	0.008905	12.651	13.287	0.636	4.39894	0.033896	452	7	106d	200		
12106392	47.4697	-6.8931	10.766	0.234	9.746	9.456	9.372	0.021	0.023	0.021	1.02	0.29	0.084	0.445283	10.6332	0.004967	10.639	11.134	0.495	4.20624	0.033508	193	3	095c	132	UX Eri *	GC,PR
14086961	293.851	5.83833	10.806	0.239	9.851	9.542	9.497	0.02	0.021	0.021	0.955	0.309	0.045	0.370319	10.6743	0.007594	10.647	11.242	0.594	4.2873	0.030697	189	3	112a	214	V0417 Aql *	GC,PR
7661848	192.84	27.2296	12.219	0.25	10.892	10.448	10.332	0.019	0.031	0.017	1.327	0.444	0.116	0.266683	12.0274	0.004223	12.021	12.595	0.574	5.2397	0.037138	228	4	058b	236	EK Com	GC,PR,RT
9233832	31.6594	14.2572	11.115	0.247	9.742	9.51	9.466	0.015	0.021	0.021	1.373	0.231	0.044	0.484974	10.9769	0.008783	10.992	11.506	0.514	3.7757	0.029274	276	4	070c	145		
8019900	267.723	29.8529	11.732	0.279	10.425	10.223	10.2	0.018	0.027	0.02	1.307	0.202	0.022	0.434212	11.5712	0.005143	11.55	12.272	0.722	3.49368	0.034593	413	7	062c	225		RT
9447688	69.1569	18.755	10.506	0.256	8.895	8.679	8.587	0.017	0.021	0.018	1.611	0.216	0.092	0.41568	10.2997	0.008888	10.3	10.924	0.624	3.58878	0.029322	220	3	073a	295	RZ Tau *	GC,PR
11768183	335.737	16.3244	11.124	0.258	10.215	9.9	9.827	0.019	0.02	0.015	0.908	0.315	0.073	0.361483	10.9953	0.005459	10.967	11.601	0.634	4.32596	0.029285	216	3	090d	302	BB Peg *	GC,PR
10653145	241.842	10.4943	12.108	0.231	10.881	10.473	10.247	0.021	0.029	0.019	1.227	0.408	0.226	0.350103	11.9919	0.008208	11.969	12.769	0.8	5.05653	0.037051	244	4	084c	227		
6734014	56.7999	25.1164	11.498	0.17	10.279	9.917	9.899	0.021	0.029	0.018	1.219	0.362	0.017	0.33266	11.4191	0.005062	11.411	12.111	0.7	4.66951	0.03694	224	4	050b	330	AH Tau *	GC,PR
890396	187.889	68.6355	12.178	0.255	10.451	9.97	9.884	0.016	0.015	0.015	1.727	0.481	0.086	0.279921	12.0475	0.00474	12.037	12.821	0.784	5.55382	0.023296	199	2	007c	573		
6715004	61.2029	33.9559	11.342	0.212	9.934	9.619	9.54	0.023	0.032	0.016	1.408	0.315	0.079	0.373044	11.2206	0.0056	11.215	11.805	0.59	4.33803	0.040692	238	5	050a	373		
5189081	234.205	47.622	12.633	0.257	11.606	11.198	11.117	0.013	0.014	0.018	1.027	0.408	0.081	0.36047	12.4974	0.003901	12.471	13.12	0.649	5.06772	0.021472	306	3	039d	371		
15956050	185.328	-13.997	11.304	0.206	10.147	9.951	9.918	0.018	0.021	0.019	1.157	0.196	0.033	0.474492	11.1662	0.004629	11.176	11.619	0.443	3.47978	0.03074	345	5	128d	119		

<sup>a</sup>Ra and Dec information are taken from the corresponding 2MASS observations, due to the better spacial resolution.  $m_R$  is the apparent ROTSE magnitude and  $\Gamma$  is given in days. Max is the average magnitude of the brightest observations and Min is the average magnitude of the dimmest. Amp is the difference between them. D is given in parsecs and Obs is the number of observations passing our loose set of cuts. Included references are to the GCVS, the Pribulla catalog and the ROTSE-I test fields.